CHAPTER 32

Reconstitution and Functional Analysis of Kinetochore Subcomplexes

Daniel R. Gestaut[*]**, Jeremy Cooper**[‡]**, Charles L. Asbury**[†]**, Trisha N. Davis**[*]**,** *and* **Linda Wordeman**[†]

[*]Department of Biochemistry, University of Washington, Seattle, Washington 98195

[†]Department of Physiology and Biophysics, University of Washington, Seattle, Washington 98195

[‡]Research Engineer, Applied Precision, Inc. Issaquah, WA 98027

Abstract

Kinetochores are multifunctional supercomplexes that link chromosomes to dynamic microtubule tips. Groups of proteins from the kinetochore are arranged into distinct subcomplexes that copurify under stringent conditions and cause similar phenotypes when mutated. By coexpressing all the components of a given subcomplex from a polycistronic plasmid in bacteria, many laboratories have had great success in purifying active subcomplexes. This has enabled the study of how the microtubule-binding subcomplexes of the kinetochore interact with both the microtubule lattice and dynamic microtubule tips. Here we outline methods for rapid cloning of polycistronic vectors for expression of kinetochore subcomplexes, their purification, and techniques for functional analysis using total internal reflection fluorescence microscopy (TIRFM).

 Daniel R. Gestaut and Jeremy Cooper contributed equally.

I. Introduction

The faithful transmission of genetic material during cell division is essential for all life. In eukaryotes, this process utilizes a large molecular machine termed the mitotic spindle. Central to the process is the kinetochore, which mediates the link between chromosomes and microtubules. The kinetochore, however, is not simply a linker. Beyond providing a physical connection, the kinetochore controls chromosome positioning, regulates its attachment to microtubules, and delays mitotic progression until properly bioriented. This multifunctional aspect is evident in its complexity with around 80 distinct proteins (Cheeseman and Desai, 2008). Because of this complexity, unraveling the roles the different proteins play and the mechanisms they use to achieve them is challenging. Here we describe methods to systematically analyze one of the most basic functions of the kinetochore, attachment to dynamic microtubule tips.

Microtubule binding assays have identified subcomplexes of the core kinetochore that bind directly to microtubules (Cheeseman *et al*., 2006; Miranda *et al*., 2005; Wei *et al*., 2007). These studies, however, only provide a static picture. The mechanism that enables kinetochores to remain attached to constantly remodeling microtubule tips where thousands of tubulin subunits are assembled and disassembled is perplexing. To address this question, we have employed advanced biophysical techniques. Through total internal reflection fluorescence microscopy (TIRFM), we have characterized how kinetochore subcomplexes interact with both the microtubule lattice and dynamic microtubule tips at the single-molecule level (Gestaut *et al*., 2008; Powers *et al*., 2009). Using a feedback-controlled optical trap, we have demonstrated that these subcomplexes can remain coupled to dynamic microtubule tips while under piconewton-scale forces similar to those experienced by kinetochores *in vivo* (Asbury *et al*., 2006; Franck *et al*., 2007; Powers *et al*., 2009). The methods used for these optical trapping measurements are described by Franck *et al*. (2010). Collectively, these functional assays illuminate the mechanisms that allow kinetochores to maintain a floating grip on microtubule tips.

In our pursuit of these goals we have improved several technologies. Here we outline methods for rapid cloning of polycistronic vectors for expression of kinetochore subcomplexes, their purification, and techniques for functional analysis using TIRFM. Although the techniques are described in the context of studying kinetochore subcomplexes, many of them could be more broadly applied to the study of other recombinant protein subcomplexes. In this chapter, a general knowledge of microtubules is assumed. For background we point the reader to the Mitchison lab website,[1] which has detailed protocols for the purification, labeling, and polymerization of tubulin. Finally, where appropriate, the Hec1/Ndc80 subcomplex is used as an example for protocols also applicable to other kinetochore subcomplexes.

II. Methods

A. Polycistronic Cloning

The number of identified kinetochore proteins has dramatically increased over the past decade to around 80. The proteins are arranged in distinct subcomplexes that copurify under stringent conditions. These subcomplexes likely represent functional

[1] http://mitchison.med.harvard.edu/protocols.html

pieces of the kinetochore as mutations in different proteins of a given subcomplex often lead to similar phenotypes. Recombinant expression of individual proteins from a given subcomplex often results in poor expression levels, low solubility, and copurification of chaperones. However, in studies where the subunits of all the proteins of a subcomplex are coexpressed from a polycistron in bacteria, functional soluble complexes have been obtained (Cheeseman *et al.*, 2006; Hori *et al.*, 2008; Kline *et al.*, 2006; Miranda *et al.*, 2005; Wei *et al.*, 2005).

A system for cloning into a polycistronic vector was developed by Tan (2001), in which genes are first cloned into a transfer vector containing upstream signals necessary for expression in the polycistron. These signals include a translational enhancer and Shine–Dalgarno sequence, which drive efficient binding and activation of ribosomes. On either end of the insertion site are a series of unique restriction sites that allow the subcloning of each gene with the flanking signals into a polycistronic vector (Fig. 1A). Planning is very important as the first gene must be cloned using the most internal restriction sites in the transfer vector and go into the first position in the polycistron, the second gene in the second position with the second set of restriction sites, etc. We have found that this approach is cumbersome, and have simplified the cloning by adding upstream signals for translation to the primer used to amplify the desired gene via PCR (Fig. 1B). This avoids the need for the transfer vector, and gives the researcher freedom to insert genes into the polycistron in any order (Fig. 1C).
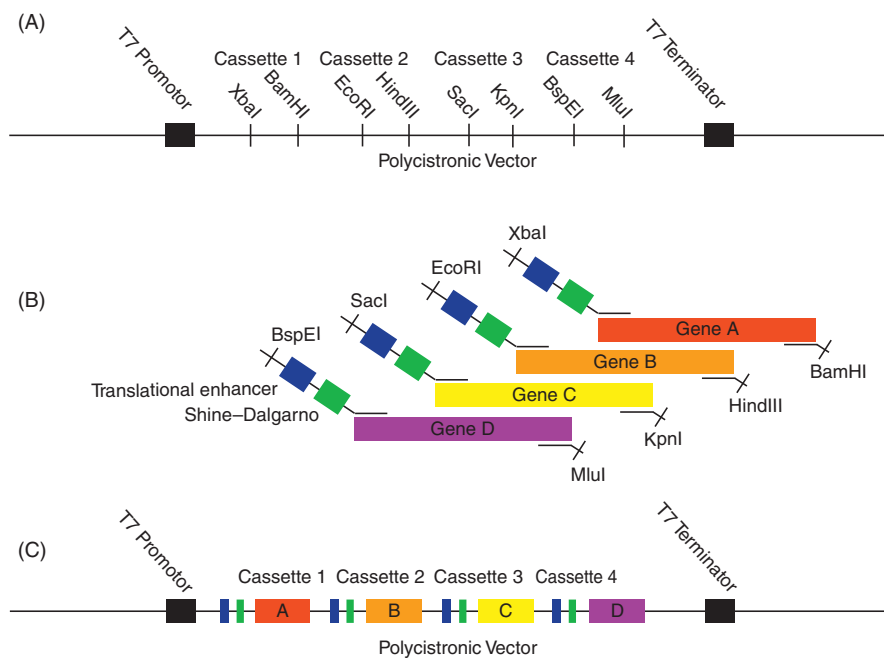
Fig. 1 Polycistronic cloning. (A) Schematic of the polycistronic vector developed by Tan *et al.* (B) Schematic of genes (multiple colors); 5′ primers containing Shine-Dalgarno sequence (green box), translational enhancer (blue box) and restriction enzyme recognition sequence; and 3′ primers with restriction enzyme recognition sequence for creating insertion products. (C) Schematic of final polycistronic vector. (See Plate no. 50 in the Color Plate Section.)

Many other considerations made during the cloning of a polycistronic vector can lead to more successful purifications. In our hands, better expression is achieved by placing the larger genes in the more 3′ cassettes of the polycistron. This may be because ribosomes are more effectively loaded, or funneled, from the shorter transcripts onto the ribosome-binding sites for the longer genes (Schoner *et al*., 1990). The affinity tag used to purify the complex should be inserted on a protein known to tolerate tags *in vivo*. Moreover, an affinity tag on the end of the protein most susceptible to degradation can allow separation of the intact protein from degraded versions. If possible, the affinity tag should be inserted on the protein expressed at the lowest levels. If all the other proteins are in excess, then any complexes containing the affinity-tagged protein should be complete. If instead the affinity-tagged protein is expressed at levels significantly greater than its binding partners, purification will result in a variety of incomplete complexes that may be difficult to separate from the complete complex. In addition to the affinity tag, we also add a restriction site for insertion of a fluorescent protein tag in frame. Again, the fluorescent tag should be inserted at a place known to be tolerated *in vivo*. Because of the size of the polycistron an 8-bp restriction site will have a greater chance of being unique to both the genes already in the polycistron and in tags to be added later.

B. Protein Expression and Purification

Many of the same considerations required for expression of individual proteins also apply to expression from polycistronic vectors. Because eukaryotic genes contain codons that are rare in bacteria, the coexpression of tRNAs for these codons is essential for robust expression. Many bacterial strains are available for this purpose. Our choice is BL21 Rosetta DE3 (Novagen/EMD Biosciences, San Diego CA), which includes an inducible T7 RNA polymerase and a plasmid that expresses both the rare tRNAs and the T7 lysozyme gene for easier lysis. For expression including proteins tagged with GFP (or its equivalents), induction at a low growth temperature (23°C) enhances folding. (Remember that GFP was originally cloned from a jelly fish collected at Friday Harbor Laboratories in Washington State, where the waters average about 10°C). Low-temperature inductions also turn on the expression of chaperones, which can aid in folding.

The polycistronic vector is particularly susceptible to recombination because it contains homologous sequences upstream of each gene. Ostensibly, genes that produce toxic products will have both the opportunity and selective pressure to be excised by homologous recombination. For this reason, it is essential to use cloning strains that lack the gene for recombinase, the *recA* gene. Most strains used for expression, however, contain a functional recombinase because its absence causes slow growth. Although we have experienced little trouble so far from recombination during expression, a recombinase-free expression strain has recently been created (Rosettablue—Novagen) and could be considered for expression.

1. Purification of the Hec1 Complex

1. Grow (2) 1 l cultures to ~20 Klett at 37°C.
2. Decrease temperature of incubator to 20°C (wait for 30 min for temperature of the culture to equilibrate).

3. Add 200 µl of 200 mg/ml isopropyl-beta-D-thiogalactopyranoside (IPTG) to induce expression and express overnight (~12 h).
4. Pellet cells at $4000 \times g$ for 10 min, resuspend in 20 ml phosphate-buffered saline (PBS) containing 1 mM phenylmethysulfonyl fluoride (PMSF), and pellet again at $4000 \times g$ for 10 min.
5. Resuspend pellets in 30 ml of lysis buffer [300 mM NaCl, 50 mM HEPES buffer, pH 7.6, Complete protease inhibitors (Roche Applied Science, Indianapolis IN), 5 U/ml Benzonase (Novagen), 10 mM imidazole, and 1 mM PMSF (Sigma-Aldrich, St. Louis MO) added just before lysis].
6. Lyse cells $2\times$ in a French press with 0.5 mM PMSF added after each lysis.
7. Clear lysate at $30,000 \times g$ for 30 min.
8. During the spin, pour a 5-ml bed volume column of talon resin (BD Biosciences, San Jose CA) and equilibrate with 300 mM NaCl + 50 mM HEPES buffer, pH 7.6.
9. Load cleared lysate onto the talon resin column at ~0.5 ml/min.
10. Wash column with 15 ml lysis buffer to inhibit any remaining proteases followed by 30 ml of 300 mM NaCl + 50 mM HEPES buffer, pH 7.6.
11. Elute bound protein with 300 mM NaCl, 50 mM HEPES buffer, pH 7.6, and 400 mM imidazole, and collect 1 ml fractions.
12. Pool and concentrate peak fractions containing the most protein (by Bradford Assay) to 1 ml using an Amicon ultra 50 kD MWCO concentrator (Millipore, Danvers MA).
13. Separate concentrated, pooled protein on an SDX200 16/60 gel filtration column (GE Healthcare Bio-Sciences, Piscataway NJ) equilibrated with 200 mM NaCl + 50 mM HEPES buffer, pH 7.6.
14. Set aside a small sample (~100 µl) of the peak fraction for determining protein concentration.
15. Add 80% glycerol to the remainder of the peak fraction to a final concentration of 10%.
16. Make small aliquots of the protein (~10 µl), snap-freeze in liquid nitrogen, and store at $-80°C$.

C. Methods for Single–Molecule Analysis of Kinetochore Subcomplexes: TIRF Microscopy

TIRFM has been used extensively to study the dynamics of interactions between proteins and polymers such as DNA, actin, and microtubules. In TIRFM, excitation lasers are aimed at an angle such that the beam is completely reflected at the interface between two mediums (usually between a coverslip and the aqueous solution within a flow channel above the coverslip). This creates an evanescent field that decays exponentially so as to preferentially excite fluorophores within ~100 nm of the coverslip. This technique eliminates background fluorescence caused by excitation of fluorophores outside the plane of focus, which would normally overwhelm the signal from individual fluorophores, providing single-molecule resolution. TIRFM, therefore, is a vital tool for characterizing how individual kinetochore subcomplexes interact with the microtubule lattice and dynamic microtubule tips.

1. TIRF Microscope Setup

To observe the interaction of kinetochore subcomplexes with microtubules, we needed a two-color TIRFM setup. We chose to use a far-red laser (FTEC-635-0-25-PFQ, Blue Sky Research, Milpitas CA) that excites either Cy5 or Alexa-647 for

visualizing microtubules with some of their subunits covalently modified with these dyes, and a blue laser (473-30, LaserPath Technologies, Oviedo FL; or, more recently, Sapphire 488-75, Coherent, Santa Clara CA) for the excitation of GFP-tagged kinetochore subcomplexes. There are three major steps required for this setup, the alignment of the two lasers before entering the microscope, the building of the TIRF microscope itself, and the capture of the images from the two laser channels. Although commercial setups are available for this application, we chose to build our own which was both cost-effective and provided greater flexibility.

To align two lasers, both the angle at which the beams are aimed and the position of the beams must be the same as they enter the microscope. Control of these parameters can be accomplished either through a series of adjustable lenses and mirrors or by the use of fiber optics, which allows both to be controlled. We chose not to use fiber optics which are more difficult to align and more susceptible to loss of alignment. The final merged beams are passed through an iris that is adjusted to allow just enough light through to excite the full field of view in the microscope. This field iris eliminates unusable light that could potentially scatter and contaminate the otherwise collimated illumination beam. Finally, the intensity of a laser beam has a Gaussian distribution, and therefore the width of the beams for both lasers should be optimized so that the change in intensity from the center of the opening in the field iris to the edge is the smallest possible (largest overall beam width), while not causing too much loss in overall beam intensity. (If the beam is widened too far, it will not be effective for exciting fluorophores.) Because the lasers we used are not perfectly monochromatic, we also added filters for each laser beam upstream of the microscope to ensure a narrow range of wavelengths for excitation.

TIRFM requires that the illumination light reaching the sample is well collimated and at an angle greater than the critical angle, such that the light undergoes total internal reflection at the coverslip/sample interface. For TIRF, the objective must have a numerical aperture (NA) greater than 1.40 and a NA > 1.45 is recommended as it allows for greater flexibility in the depth of the evanescent field that illuminates the sample at the coverslip surface. (Currently, we use a Nikon objective, CFI Planapo-chromat 100× 1.49 NA.) The light striking the interface must be collimated otherwise the illumination beam will have a range of incidence angles leading to a less defined depth of field. To accomplish this, the beam is brought to a tight focus (a "waist") at the back focal plane of the objective (for TIRF objectives this is usually just 2–3 mm from the front surface of the objective). Each objective will have its own parameters for alignment; however, one requirement that is almost universally true is that the final lens that focuses the illumination beam at the back focal plane should be as close as possible to the objective (150 mm or less). This ensures a tightly focused beam at the back focal plane (and thus a tightly collimated beam leaving the objective).

As mentioned earlier, the depth of the evanescent field created by the TIRFM scope is dependent upon the angle of incidence. This angle is dependent on the NA of the objective and how far from the centerline of the objective the illumination beam is focused. (The further from the centerline the greater the angle of incidence and shorter the depth of the evanescent field). For this reason, it is desirable to be able to control this distance. This can be accomplished by mounting a mirror into a translatable stage that can be externally controlled and a system of three lenses that maintain these translations while keeping the beam waist focused at the back focal plane of the objective (Fig. 2). Two of these lenses downstream of the mirror
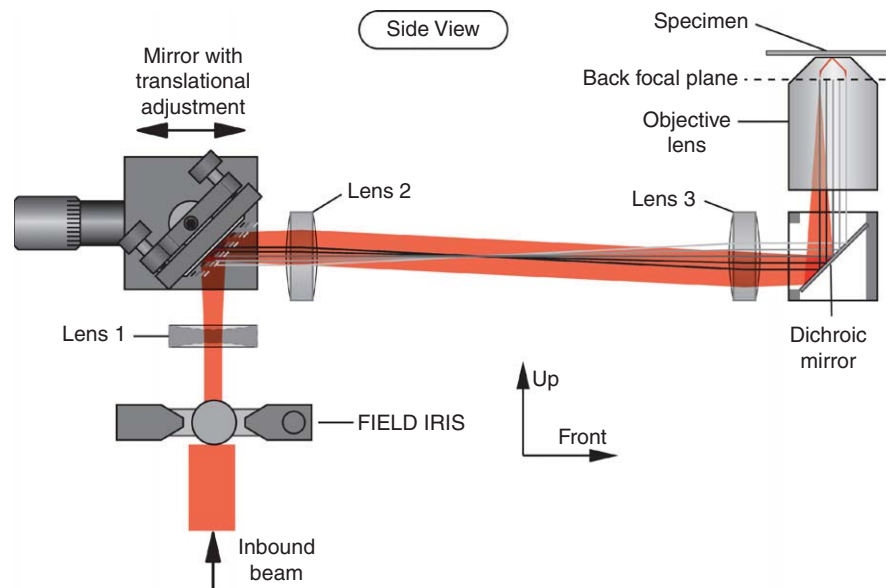
Fig. 2 TIRFM depth control. Schematic of the system that allows control of the depth of the TIRF field. In this system movement of the mirror will result in a displacement in the point of focus on the back focal plane. This movement ultimately results in a change in the depth of the TIRF field. (See Plate no. 51 in the Color Plate Section.)

compose a Keplerian telescope so that the translation of the mirror, which will initially be converted to angular diffractions by the first lens, is converted back to a translation by the second lens. The third lens, which is upstream of the translatable mirror, causes the collimated beam to diverge prior to reaching the first lens downstream of the mirror; this is required so that the beam leaving the final lens is focused at the focal plane, and not collimated at the focal plane.

To simultaneously collect images from both the far-red and green channels, we implemented a system that allowed both images to be projected side by side onto a CCD camera (iXon 887-BI, Andor Technology, Belfast, UK) (Fig. 3). Although using a second camera would simplify the optical layout, the cameras are relatively expensive. Since the CCD is square, the first step was to pass the image leaving the microscope through an aperture that created a rectangular border at its plane of focus so that the component images would fit side by side onto the CCD. We next developed a system that utilizes two dichroic mirrors to split and rejoin the two separately colored images side by side onto the same camera CCD. The images are refocused using separate lenses within each path and each image also passes through an additional emissions filter. Because the images have slightly different path lengths, one image ends up being slightly magnified relative to the other. To avoid this problem an additional lens was added to the red path, which, in conjunction with the other lens, allowed both the focus and magnification to be controlled independently.

2. Procedure for Making Slides and Coverslips

    a. Coverslip Silanization.   The major advantage of TIRFM stems from the elimination of background fluorescence. Because this requires imaging close to the
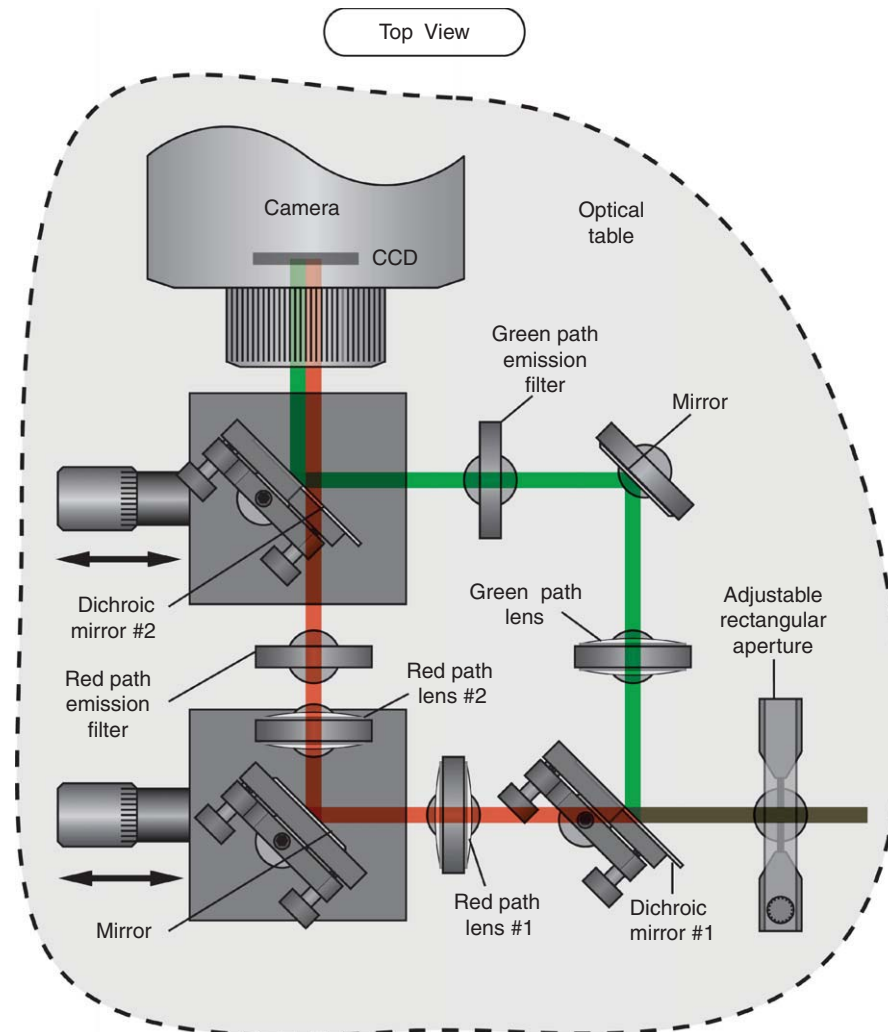
Fig. 3 Simultaneous two-color imaging system. This system utilizes two dichroic mirrors to split and rejoin the two separately colored images side by side onto the same camera CCD. The images are refocused using separate lenses within each path. (See Plate no. 52 in the Color Plate Section.)

coverslip surface, it is essential to minimize adsorption of fluorescently labeled protein to this surface. Nonspecifically bound fluorescent molecules and aggregates make interactions with the microtubules difficult to distinguish from background binding. Transient nonspecific interactions with the coverslip can also affect diffusion rates, on-rates, and off-rates. To avoid these issues the coverslips must be thoroughly cleaned and silanized. During silanization, silane molecules react with the glass surface and each other forming a covalently linked layer above the coverslip surface. The silane used is a functionalized form that has a linked group (in our case a short chain PEG) that ends up pointed away from the glass surface creating a hydrophilic environment at the coverslip surface in the perfusion chamber. The

coverslips are dried under a steady flow of high-purity nitrogen gas as silane reacts with oxygen. Silanized coverslips may also be stored under an inert gas such as nitrogen. Below we outline our protocol for coverslip silanization adapted from Cras et al. (1999) and Walba et al. (2004). Custom Teflon racks that have minimal contact points with the coverslips are used as Teflon can tolerate the various surface treatments.

1. Load 13 22 mm × 60 mm coverslips into each of 4 custom Teflon racks (for a total of 52 coverslips).
2. Rinse racks under distilled water and then rinse 1× in a 500-ml beaker of ddH$_2$0.
3. In a fume hood, pour ~160 ml methanol into a clean 500 ml flask (use a glass funnel). Then pour ~160 ml concentrated HCl (37%) into the flask and mix well. The solution will heat up a bit, so place on ice for about 10 min to reduce fuming.
4. Slowly pour the 50/50 HCl/methanol solution into a 600-ml Berzelius beaker.
5. Remove the coverslips from the ddH$_2$0 rinse and thoroughly shake off any excess water
6. Slowly lower the coverslips into the Berzelius beaker containing the 50/50 HCl/methanol solution. Raise and lower the coverslips a few times to ensure that the residual rinse water clinging to the coverslips and Teflon racks is well mixed in with the acid wash. Incubate for 30 min.
7. While incubating, prepare five clean 600-ml beakers with 400–500 ml of ddH$_2$0 each for rinsing coverslips.
8. When HCl/methanol incubation is finished, rinse the coverslips by vigorously dipping several times into each of the five rinse beakers.
9. In order to verify that the acid is effectively being rinsed off, check the pH of the rinse beakers by pipeting a few microliters onto pH strips. By the third rinse, the pH should be near the original pH of the ddH$_2$0. The pH of the fourth and fifth rinse beakers should be indistinguishable from the original pH of the ddH$_2$0.
10. Prepare a sulfuric acid wash by pouring 300 ml of concentrated sulfuric acid (95–98%) directly into a 600-ml Berzelius beaker.
11. Remove the coverslips from the final ddH$_2$0 rinse and thoroughly shake off any excess water.
12. Slowly lower the coverslips into the Berzelius beaker containing the sulfuric acid. Raise and lower the coverslips a few times to ensure that the residual rinse water clinging to the coverslips and Teflon racks is well mixed in with the acid wash. Incubate for 30 min.
13. While incubating, prepare seven clean 600-ml beakers with 400–500 ml of ddH$_2$0 each for rinsing coverslips. Note the additional rinse beakers are required to fully remove the sulfuric acid.
14. When sulfuric acid incubation is finished, rinse the coverslips by vigorously dipping several times into each of the seven rinse beakers.
15. In order to verify that the acid is effectively being rinsed off, check the pH of the rinse beakers.
16. Remove the coverslips from the final ddH$_2$0 rinse and thoroughly shake off any excess water.
17. Lower coverslips into a clean 600-ml Berzelius beaker and cover with a stopper.
18. Dry coverslips under dry N$_2$ at about 5 l/min flow rate for about 1 h.

19. After the coverslips have been completely dry for at least 15 min, mix up the following silanization solution in a 500-ml flask:
    a. 320 ml toluene.
    b. 5.6 ml 2-methoxy(polyethyleneoxy)propyltrimethoxysilane (SIM-6492.7, Gelest, Morrisville PA).
    c. 2.0 ml butylamine.
20. Remove stopper and slowly pour the silanization solution into the 600-ml Berzelius beaker containing the coverslips. Replace stopper, turn dry N_2 flow rate down to about 1 l/min, and incubate 90 min.
21. Remove the coverslips from the silanization chamber and thoroughly shake off any excess silanization solution.
22. Rinse the coverslips by vigorously dipping several times into each of two toluene-filled rinse beakers. Thoroughly shake off excess solution after each rinse.
23. Place coverslips back into a clean 600-ml Berzelius beaker and cover with a stopper.
24. Dry coverslips under dry N_2 at about 5 l/min flow rate for about 30 min.
25. When the coverslips are completely dry, place each of the four separate coverslip racks into separate glass tubes for overnight cure. Place Teflon stoppers on each of the individual curing chambers and turn dry N_2 flow rate down to about 1.5 l/min.
26. Cure overnight and store under dry N_2.

   b. Slide Design.   As mentioned before, when studying complexes at single-molecule resolution, small variations in the experimental setup can significantly alter the data. Factors that can vary between slides are as follows:

– the quality of the silanization of the coverslip which will affect the amount of background binding observed.
– the depth of the TIRF field; this is optimized between slides to get the best signal-to-noise ratio.

Because of these inherent variations, the experimental and control measurements should be done on the same slide. We have developed a slide design using standard disposable glass slides and coverslips that allows the generation of four perfusion chambers. The perfusion chambers are attached to a peristaltic pump to control the flow rate of buffers through the chambers and to achieve complete buffer exchange. Below we outline our protocol to produce four perfusion chambers per coverslip:

1. Glass slides (Gold Seal, Thermo Fisher Scientific, Waltham MA) are drilled to produce eight holes, four along each side of the long axis (Fig. 4A, light arrowheads).
2. Double-sided sticky tape (Scotch) is placed between these holes across the short axis (Fig. 4A, dark arrowhead), and a silanized coverslip is placed on the other side of the tape to produce four perfusion chambers (Fig. 4B).
3. Using cotton swabs, the ends of the perfusion chambers are sealed with grease up to the holes in the slide (Fig. 4C, arrowheads). Ethanol is used to wipe away excess grease.
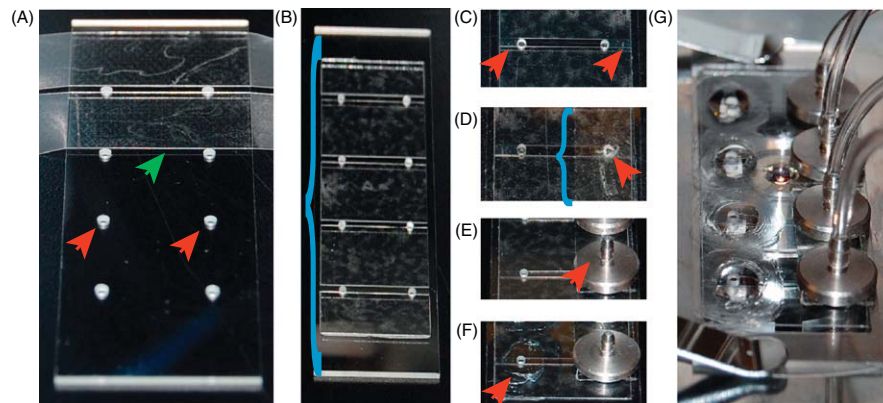
Fig. 4 Four perfusion chamber slide. (A) Glass slide with four holes (red arrowheads) drilled along each long axis, holes are spaced to allow double-sided sticky tape (green arrowhead) to be placed between them. (B) One silanized coverslip (blue bracket) is placed onto the double-sided sticky tape, and excess tape is removed. (C) Grease is used to seal the edges of the perfusion chambers (red arrowheads) up to the holes in the slide. (D) The slide is flipped over and rubber adhesive transfer tape (blue bracket) is placed above the holes along one long axis of the slide. A hole (red arrowhead) is created in the adhesive transfer tape above the hole in the slide using forceps. (E) Custom flow adapters (red arrowhead) are attached to the slide via the adhesive transfer tape. (F) Rings of grease (red arrowhead) are made around the holes opposite the flow adapters to create a pool for buffers. (G) Image of the final slide on the microscope with outlet tubing attached to the flow adapters. (See Plate no. 53 in the Color Plate Section.)

4. The slide is flipped such that the coverslip is now underneath the slide. Adhesive transfer tape (3M F9473PC) is placed along one set of four holes, and a hole in the transfer tape above the hole in the slide is produced with forceps (Fig. 4D, arrowhead).

5. Adapters are placed onto the adhesive transfer tape above each of the holes to allow attachment of a peristaltic pump (Fig. 4E).

6. Above the remaining four holes, a ring of grease is made to produce a pool for buffers that will be pulled through the perfusion chamber (Fig. 4F).

c. Attachment of Microtubules to the Coverslip. In TIRFM the area of experimentation is directly above the coverslip, so the experiment must be performed in this narrow depth of field. Directly adsorbing the microtubules to the glass slide will inhibit the action of some microtubule enzymes, notably microtubule depolymerases, and make it impossible to measure the behavior of dynamic microtubules. To restrict the microtubules to the evanescent field without directly adsorbing them to the glass, the microtubules must be tethered to the coverslip. The best method would employ a molecule that is inert to free tubulin but would rapidly tether dynamic extensions off of microtubule seeds during imaging. This will prevent the microtubule ends from "flopping" out of the evanescent field during imaging. We have used two methods, both of which take advantage of nonspecific adsorption of proteins to the coverslip. Although the silanization process we use has been carefully optimized, imperfections still exist creating spots where proteins can be nonspecifically and permanently adsorbed to the coverslip. The ratio of the tethering agent to a blocking protein

(such as BSA) that can compete for binding to the imperfections is optimized to control the density of the tethering agent on the coverslip. To minimize the amount of tubulin subunits interacting with tethering agents, and maximize the accessibility of the microtubule lattice, the minimum amount of tethering agent density is used that still prevents movement of parts of the bound microtubules in and out of the narrow field of excitation above the coverslip. The first method uses a biotin–streptavidin–biotin linkage, while the second method uses a modified kinesin that binds to microtubules in a rigor state and does not release them in the presence of ATP/GTP (Rice *et al*., 1999).

Method 1:

1. Biotinylated κ-casein is allowed to bind to the imperfections in the silanization.
2. Free biotinylated κ-casein is washed away in two washing steps.
3. Strepavidin is linked to the biotinylated κ-casein, followed by another set of washes to remove the free streptavidin.
4. Microtubules that have a small proportion of their tubulin subunits (1:70) biotinylated are linked to the streptavidin.

Method 2:

1. Purified rigor kinesin is adsorbed to the imperfections in the silanization.
2. Free rigor kinesin is washed away, and microtubules are bound.

The second method is quicker and has the advantage that rigor kinesin only interacts with polymerized tubulin and therefore dynamic extensions are bound down (free biotinylated tubulin saturates streptavidin sites faster than polymerization of the tubulin, which prevents dynamic extensions from becoming tethered to the coverslip). A disadvantage of the second method is that the coiled-coil domain of the rigor kinesin can cause increased nonspecific interactions with the subcomplex being studied; to minimize these we use the lowest concentration of rigor kinesin that still prevents "floppiness" in the microtubules.

3. Experimental Protocol to Study Interaction Between Kinetochore Subcomplexes and Microtubules

a. Optimization of Conditions. In single-molecule studies, small changes in conditions can significantly alter the outcome of the experiment. We first optimize our buffers to prevent nonspecific binding. Nonspecific binding is detrimental in that it causes loss of your protein changing the actual working concentration (which can be significant when working at pM concentrations), and also speckles the background of your field of view making data analysis difficult. Dynamic parameters such as rate constants and diffusion coefficients can be altered by nonspecific interactions with the experimental setup. To prevent nonspecific binding we use blocking proteins such as BSA and κ-casein, which saturate imperfections in the coverslip silanization. Salt can also drive nonspecific hydrophobic interactions, and decreasing the ionic strength of the solution can help prevent these. Effective conditions for preventing nonspecific interactions seem to differ between complexes, and therefore must be optimized empirically. After finding an appropriate buffer, the concentration of the complex must also be optimized for single-molecule studies.

When concentrations are too low, binding events are infrequent, while at higher concentrations binding events (especially if diffusive) may overlap preventing their analysis. The on-rate and off-rate can be adjusted by complex concentration and ionic strength. Finally, the optimal situation for studying subcomplexes requires a uniform species, and therefore, conditions in which your complex exists in a near-homogeneous state should be identified if possible (i.e., monomer, dimer etc.).

The simplest TIRF assay uses microtubules stabilized by paclitaxel. Prior to the assays, microtubules are assembled with a 1:100 ratio of Alexa-647 labeled to unlabeled tubulin subunit for visualization. After polymerization microtubules are stabilized by the addition of paclitaxel, pelleted, and then resuspended in BRB80 with paclitaxel. This pelleting step removes the unpolymerized tubulin, which can interact with the subcomplexes being studied during TIRFM. The microtubules are bound to the coverslip as described above, washed with BRB80 plus a blocking protein, and washed again with BRB80 plus a blocking protein and free-oxygen scavenger system to slow photobleaching.

b. Protocol for Analysis of Interaction of Subcomplexes with Paclitaxel Stabilized Microtubules.

Steps listed are for all perfusion chambers, and during any incubation step the solution for the next step should be applied to the well to prevent the well from drying.

1. Wash with 100 µl of dH$_2$O three times.
2. Flow in 15 µl of rigor kinesin with BRB80 containing 8 mg/ml BSA (BB80) and incubate for 5 min for surface adsorption to occur. Actual kinesin dilution ratio should be optimized to be lowest concentration that prevents flopping microtubules and will vary between rigor kinesin purifications and silanized coverslip preparations. We find a 1:100 dilution of our purified protein is a good starting point.
3. While rigor kinesin is binding focus the microscope.
4. Wash with 50 µl BB80, followed by 50 µl BB80 containing 10 µM paclitaxel (BB80T).
5. Flow in 15 µl paclitaxel-stabilized Alexa-647-labeled microtubules and allow to bind until optimal surface density is achieved. (Note that small segments of the microtubules will be anchored before complete binding of the entire polymer. During the next wash step the rest of the stabilized microtubule polymer will be anchored.)
6. Wash with 50 µl BB80T, followed by 50 µl BB80T containing free-oxygen scavengers.
7. Flow in 10 pM GFP–Ndc80 complex in BB80T containing free-oxygen scavengers.

### c. Protocol for Analysis of Interaction of Subcomplexes with Dynamic Microtubules.

1. Steps listed are for all perfusion chambers.
2. Wash with 100 µl of dH$_2$O three times.
3. Flow in 15 µl of rigor kinesin 1:30 in BB80 and incubate for five min for surface adsorption. A greater amount of rigor kinesin is required for dynamic microtubule assays for binding of the microtubule extensions in the presence of free tubulin.
4. While rigor kinesin is binding, focus the microscope.
5. Wash with 50 µl BB80, followed by 50 µl BB80 containing 1 mM GTP (GB80).
6. Flow in 15 µl Alexa-647-labeled GMPCPP stabilized microtubule seeds in GB80 and allow to bind until optimal surface density is achieved (note that the

GMPCPP seeds are small and that long extensions will be grown from them, the ratio of Alexa-647 label can also be varied so that GMPCPP seeds can be distinguished from the dynamic extensions).

7. Wash with 50 µl GB80, followed by 50 µl GB80 containing 1 mg/ml tubulin (1:100 Alexa-647 labeled to unlabeled) and free-oxygen scavengers, and let microtubules polymerize to desired length.

8. Flow in 100 pM GFP–Ndc80 Complex in BB80 containing free-oxygen scavengers.

4. TIRFM Data Analysis

The raw data from TIRF microscopy are a stack of TIFF files. Movies are collected at 10 frames per second normally for 200 seconds. As described above, two images are projected onto the camera, on the top half is the green channel, and on the bottom half is the far-red channel. To analyze the raw data we have developed a series of three programs in Labview, which correspond to three separate analysis steps. In the first step, the far-red channel is translated to overlap with the green channel, allowing the position of the microtubules to be seen in reference to the kinetochore subcomplex being studied. This allows the position of the microtubule to be traced by the user with a multi-segment line onto the green channel (Fig. 5A), and a kymograph is generated by summing the brightness of the four pixels above and below the line. In step 2, the user identifies binding events in the generated kymograph, and draws a line along the kymograph where the binding event occurs.
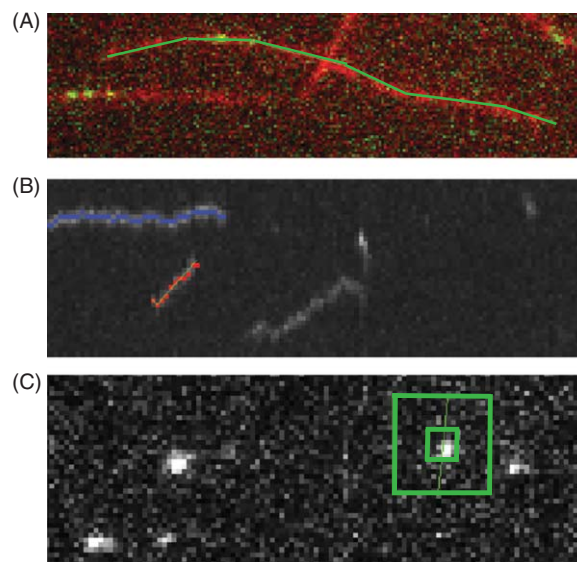
Fig. 5 TIRF data analysis. (A) Images from the red and green channels are overlapped and a multi-segmented line (green) is drawn along one of the microtubules. (B) Kymograph generated from step one, showing a preselected event (blue), currently selected event (green line, and red spots) and unselected events (grayscale). (C) Single image from the original tiff stack of the green channel (grayscale) in which a small box (green) is used to generate a brightness measurement, and a larger box (green) is used to generate a background measurement. (See Plate no. 54 in the Color Plate Section.)

The line is automatically adjusted to lie on the brightest pixel within five pixels of the line drawn by the user, and frames where the brightness does not surpass a defined threshold are omitted (Fig. 5B). Finally, in step 3 the coordinates obtained in step two are used in the original TIFF stack and the brightest pixel within six pixels of this coordinate is identified. Around this pixel a 6×6 box is drawn and a brightness measurement is made by summing the pixels. To account for background fluorescence, an additional 20×20 box is drawn around the pixel and the average brightness of these pixels excluding the inner 6×6 box is used as a measurement of background per pixel (Fig. 5C). From step 3 a file for each binding event is created containing the position, brightness, and background brightness for each frame. The binding events are then loaded into Igor for quantification and further analysis.

Plots of brightness versus frame number are created for each binding event allowing the start and end times of the event to be confirmed, and bleach steps to be identified. From these values we generate a histogram of residence times. This distribution is often well described by a single exponential decay except for the lowest bin, where events are likely missed due to the finite time resolution of the instrument. The mean from the best-fit exponential (excluding the lowest bin), or equivalently, its time constant, τ, is inverted to give the off-rate, $k_{off} = \tau^{-1}$ (e.g., in s^{-1}). For each binding event, we also calculate a mean squared displacement along the microtubule long-axis, $\langle x^2 \rangle$, for every possible time lag, Δt. The $\langle x^2 \rangle$ values are averaged across many events to generate a plot of $\langle x^2 \rangle$ versus Δt for a population. With this method, individual events contribute no more than one value to the population $\langle x^2 \rangle$ at a particular Δt, so long events are not weighted disproportionately. The one-dimensional diffusion coefficient, D, is then computed from the slope, m, of a linear fit to the plot according to $D = \frac{1}{2} m = \frac{1}{2} \langle x^2 \rangle \Delta t^{-1}$ (Berg, 1993).

A second-order on-rate can also be calculated from the TIRF data. We do this by counting the number of binding events that occur per micron of microtubule lattice over a set period of time (e.g., in $\mu m^{-1} s^{-1}$) and then converting to a second-order on-rate, k_{on} (in $M^{-1} s^{-1}$), by dividing by the total concentration of Ndc80 complex and by the total number of tubulin dimers per micron of microtubule lattice ($1585 \, \mu m^{-1}$, assuming a 13-protofilament microtubule). This calculation gives a good approximation to the second-order on-rate if four criteria are met. First, the total concentration of Ndc80 must be well below the equilibrium dissociation constant, K_d, to ensure that binding does not significantly deplete the pool of free complexes. Second, only a small fraction of lattice sites on the microtubules must be occupied, so binding does not significantly deplete the availability of sites. Third, Ndc80 loss to nonspecific background binding (e.g., to tube walls, etc.) must be negligible. Fourth, the linkage of the microtubules to the coverslip must not block a significant fraction of lattice sites. The first two criteria are usually true given the very low concentrations used to obtain single molecule resolution. However, the last two are more difficult to prove, so these calculations must be seen as approximations. We also note that the apparent on-rate can be reduced by the "missing event problem" mentioned above (i.e., some short-lived events, with residence times comparable to the temporal resolution of the instrument, will inevitably be missed). If the residence times are distributed exponentially, the magnitude of this effect can be estimated and, in principle, corrected for by comparing the number of short-lived events scored with the number predicted based on an exponential fit to the distribution.

III. Conclusion

We have outlined methods for the cloning, purification, and functional analysis of kinetochore subcomplexes. In the first section, we discuss methods for rapid cloning of a polycistron and ways to enhance protein expression. Next, we describe our design of a two-color TIRF microscope setup. Finally, we describe experimental designs for TIRFM assays and optimizations to drive reproducibility and rapid data collection. The TIRFM assays described here are quite powerful for characterizing the interactions of subcomplexes with microtubules. Although not described here, the assays may also be used to determine stoichiometry and arrangements of larger assemblies, which should prove useful as more of the kinetochore is reconstituted. Finally, we note that the optical trap is another powerful tool for assaying the strength of these interactions, which we describe in Methods section (Franck *et al.*, 2010).

References

Asbury, C. L., Gestaut, D. R., Powers, A. F., Franck, A. D., Davis, T. N. (2006). The Dam1 kinetochore complex harnesses microtubule dynamics to produce force and movement. *Proc. Natl. Acad. Sci. U.S.A.* **103**, 9873–9878.

Berg, H. C. (1993). "Random Walks in Biology." Princeton University Press, Princeton, NJ.

Cheeseman, I. M., Chappie, J., Wilson-Kubalek, E., Desai, A. (2006). The conserved KMN network constitutes the core microtubule-binding site of the kinetochore. *Cell* **127**, 983–997.

Cheeseman, I. M., and Desai, A. (2008). Molecular architecture of the kinetochore-microtubule interface. *Nat. Rev. Mol. Cell Biol.* **9**, 33–46.

Cras, J. J., Rowe-Taitt, C. A., Nivens, D. A., Ligler, F. S. (1999). Comparison of chemical cleaning methods of glass in preparation for silanization. *Biosens. Bioelectron.* **14**, 683–688.

Franck, A. D., Powers, A. F., Gestaut, D. R., Gonen, T., Davis, T. N., Asbury, C. L. (2007). Tension applied through the Dam1 complex promotes microtubule elongation providing a direct mechanism for length control in mitosis. *Nat. Cell Biol.* **9**, 832–837.

Franck, A. D., *et al.* (2010). Direct physical study of kinetochore-microtubule interactions by reconstitution and interrogation with an optical force clamp. *Methods* In Press.

Gestaut, D. R., Graczyk, B., Cooper, J. Widlund, P. O., Zelter, A., Wordeman, L., Asbury, C. A., Davis, T. N. (2008). Phosphoregulation and depolymerization-driven movement of the Dam1 complex do not require ring formation. *Nat. Cell Biol.* **10**, 407–414.

Hori, T., Okada, M., Maenaka, K., Fukagawa, T. (2008). CENP-O class proteins form a stable complex and are required for proper kinetochore function. *Mol. Biol. Cell* **19**, 843–854.

Kline, S. L., Cheeseman, I. M., Hori, T., Fukagawa, T., Desai, A. (2006). The human Mis12 complex is required for kinetochore assembly and proper chromosome segregation. *J. Cell Biol.* **173**, 9–17.

Miranda, J. J., Wulf, P. D., Sorger, P. K., Harrison, S. C. (2005). The yeast DASH complex forms closed rings on microtubules. *Nat. Struct. Mol. Biol.* **12**, 138–143.

Powers, A. F., Franck, A., Gestaut, D., Cooper, J,. Gracyzk, B., Wei, R., Wordeman, L., Davis, T. N., Asbury, C. L. (2009). The Ndc80 kinetochore complex forms load-bearing attachments to dynamic microtubule tips via biased diffusion. *Cell* **136**, 865–875.

Rice, S., *et al.* (1999). A structural change in the kinesin motor protein that drives motility. *Nature* **402**, 778–784.

Schoner, B. E., Belagaje, R. M., Schoner, R. G. (1990). Enhanced translational efficiency with two-cistron expression system. *Meth. Enzymol.* **185**, 94–103.

Tan, S. (2001). A modular polycistronic expression system for overexpressing protein complexes in *Escherichia coli*. *Protein Expr. Purif.* **21**, 224–234.

Walba, D. M., Liberko, C., Korblova, E., Farrow, M., Furtak, T., Chow, B., Schwartz, D., Freeman, A., Douglas, K., Williams, S., Klittnick, A., Clark, N. (2004). Self-assembled monolayers for liquid crystal alignment: Simple preparation on glass using alkyltrialkoxysilanes. *Liq. Cryst.* **31**, 481–489.

Wei, R. R., Sorger, P. K., Harrison, S. C. (2005). Molecular organization of the Ndc80 complex, an essential kinetochore component. *Proc. Natl. Acad. Sci. U.S.A.* **102**, 5363–5367.

Wei, R. R., Al-Bassam, J., Harrison, S. C. (2007). The Ndc80/HEC1 complex is a contact point for kinetochore-microtubule attachment. *Nat. Struct. Mol. Biol.* **14**, 54–59.